Thermodynamics of linear and star polymers at fluid interfaces

Tseden Taddese, Paola Carbone[*]

School of Chemical Engineering and Analytical Science,
The University of Manchester, Oxford Road, Manchester M13 9PL, UK

David L. Cheung[§]

Department of Chemistry, University of Warwick, Coventry, CV4 7AL, UK and
Department of Pure and Applied Chemistry,
University of Strathclyde, Glasgow, G1 1XL, UK

Corresponding authors
[*] paola.carbone@manchester.ac.uk
[§] david.cheung@strath.ac.uk

Abstract

Performing molecular dynamics simulations on model systems we study the structural changes and thermodynamic stability of polymers of varying topology (linear and star-shaped) at interface between two liquids. We find that homopolymers are attracted to the interface in both good and poor solvent conditions showing that they are surface active molecules even though not amphiphilic. In most cases changing polymer topology had only a minor effect on the desorption free energy. A noticeable dependence on polymer topology is only seen for relatively high molecular weight polymers at interface between two good solvents. Examining separately the enthalpic and entropic components of the desorption free energy suggests that its largest contribution is the decrease in the interfacial free energy caused by the adsorption of the polymer at the interface. Finally we propose a simple method to qualitatively predict the trend of the interfacial free energy as a function of the polymer molecular weight.

1. Introduction

The behaviour of polymers at a liquid/liquid interface has become increasingly technologically important in recent years. For example, many of the self-assembly processes involving macromolecules occur at such interfaces [1, 2] and the stability of micro- and nano-emulsions are determined by an efficient migration of polymers (or surfactants) towards the boundaries between the two solvents. Chemical reactions can also be carried out at a liquid/liquid interface, as for example in some types of polymerisation reactions (typically a condensation reaction) [3] or to functionalise the macromolecule itself [4]. Moreover, one of the most common chemical processes used to produce polymer nanoparticles especially for medical applications −the solvent displacement method− exploits the varying solubility of polymers in different solvents. The process involves the diffusion of the polymer chains from a good solvent, where the polymer initially dissolves, to a non-solvent where the nanoparticles are formed [5, 6]. Finally, polymer-based drug nanocarriers (either nanoparticles or micelles) are becoming increasingly popular in drug delivery. Therefore their behaviour at fluid interfaces (such as a lipid/water boundary) should be properly understood in order to predict their biological activity [7, 8].

As organic synthesis advances it is becoming possible to create macromolecules with more complex architectures than simple linear polymers, including star or ring polymers and dendrimers. [9] In particular star polymers have attracted particular attention due to their unique structure and relatively easy synthetic route [9]. They show a range of different behaviours, both in bulk solution and at interfaces, and have found use in areas such as organic electronics [10] and drug delivery [11]. The use of hyper-branched polymers in interfacial science is also becoming popular, as it is generally thought that the presence of side chains should enhance the adhesion and mobility of polymers on interfaces (mainly solid). However, it has recently been shown that the interfacial adhesion of branched polymers is significantly improved only if a complicated topology of the macromolecule is coupled with a strong molecular bond with the surface [12].

While the behaviour of polymers at solid interfaces has been extensively studied [13, 14], the behaviour of polymers at fluid interfaces has been less thoroughly investigated, despite its technological importance. In fact, the adsorption of polymers at a liquid/liquid interface is different from that at a solid/liquid one as the macromolecule penetrates both phases proportionally to their solubility. Furthermore, if the two solvents are immiscible, it is expected that the presence of the polymer lowers the interfacial tension by screening the unfavourable interactions between the two solvents. [15] The few theoretical works present in the literature support this idea. Halperin and Pincus [16] have used a mean field approach to investigate a ternary system of a monodisperse polymer at a liquid/liquid interface and found

that homopolymers may indeed be attracted to the interface. The authors suggested that responsible for this attraction was the presence of the polymer monomers between the two solvents which lowered the free energy of the system. Along with theoretical work, computer simulations can also help in understanding the thermodynamic stability of nano-objects at fluid interfaces and correlate it with the structural changes occurring in the system. For example, recent simulations of a model system have shown that uniform dendrimers interact strongly with liquid-liquid interfaces. [17] The interaction is similar to that previously found for nanoparticles [18]; specifically the interaction range is significantly larger than it would be expected from simple consideration of the dendrimer size and the desorption free energy was similar to that calculated for nanoparticles of comparable size. Moreover, when the dendrimer is functionalised with end groups with different affinities for the two solvent components the interfacial stability increases. The stability also increased when a core-shell structure was considered. The dendrimer also undergoes significant changes in shape, going from spherical in bulk solution, to disk-like at the interface, and adopting an elongated cigar-like structure at intermediate separations. These studies also demonstrated that the use of a generic bead-spring model for such simulations can provide results relevant to experimental systems (for example the observed shape change in the bead-spring dendrimer model was similar to that seen in atomistic simulations of PAMAM dendrimers at the air-water interface [19]) opening the possibility of developing a generic theoretical framework valid for any macromolecular system irrespectively of its chemical composition.

The aim of this work is to investigate how the interfacial stability of polymers is affected by the molecular weight and the topology of the chain. Moreover, we seek a relation which could predict the tendency of a polymer to diffuse into one of the two solvents as a function of its molecular weight and solvent quality. As in previous work [17] we use molecular dynamics simulations employing a bead-spring representation of the polymer and model the solvent as a binary Lennard-Jones mixture. Different lengths of linear polymers are studied in order to investigate the effect of molecular weight on the adsorption strength. Star polymers of different functionalities are also modelled to address the effect of polymer topology on the interfacial adsorption. By keeping the number of beads in the star polymers constant we aim to isolate the effect of changing the polymer topology, whilst changing the polymer-solvent interactions allows us to study how the interfacial behaviour is affected by the solvent quality.

Following this introduction we outline the simulation model and methodology employed in this work. We then present the results, focusing first on the interaction between polymer and interface as a function of chain topology and size and solvent quality. Next we will discuss the separate contributions to the stability of macromolecules at liquid interfaces, and examine

the relationship between the properties of polymers in bulk solution and their adsorption. Finally we present some conclusions and possible avenues for further work.

2. Model and methodology

In order to determine the effect of topology on the adsorption of polymers at a liquid-liquid interface, simulations were performed on both linear and star polymers. For the linear polymer chain model, the number of monomers was varied from 25 to 90. A comparison was then made with four star polymer models with the same (or similar) number of monomers as two linear ones. Within the star polymer models, the functionality was also varied: while the total number of monomers was kept constant their arrangement and the number and length of arms varied. For the remainder of this paper the linear polymers will be referred to as Lx, (where x is the number of monomers) and the star polymers as NyLx (where y is the number of arms and x is the arm length). The models used in the simulations are summarised in Table 1.

Model label	$\mathbf{N_m^{tot}}$	$\mathbf{N^a}$	$\mathbf{N_m^a}$
L25	25	1	--
L40	40	1	--
L50	50	1	--
L60	60	1	--
L70	70	1	--
L80	80	1	--
L90	90	1	--
N4L6	25	4	6
N6L4	25	6	4
N11L6	67	11	6
N6L11	67	6	11

Table 1. Summary of all the models used, along with the total number of monomers, N_m^{tot}, the number of arms, N^a , and the number of monomers in each arm, N_m^a .

As in previous work the simulated systems consisted of a single polymer solvated in a binary mixture. [17] The solvent was modelled as a two-component liquid, interacting through a cut and shifted Lennard-Jones potential

$$V_s(r) = \begin{cases} 4\varepsilon\left[\left(\frac{\sigma}{r}\right)^{12} - \left(\frac{\sigma}{r}\right)^{6}\right] - V_c & r < r_c \\ 0 & r > r_c \end{cases} \qquad \text{(eq. 1)}$$

where r_c = 2.5σ and $2^{1/6}$σ for interactions between like and unlike components respectively, and V_c is the interaction energy at the cut-off. For most simulations 24000 solvent beads (12000 of each component) were used but for the longest polymer chain a larger box of around 40000 solvent beads were used, in order to avoid interaction with the period image. Throughout this paper, all the simulation results are reported in LJ reduced units. The values of the potential well depth, ε, the diameter of the bead, σ, and the solvent bead mass, m, are used to define the system units for the energy, length and mass respectively. The reduced temperature and pressure, $T^*$and P^*, are given by $T^*=k_BT/\varepsilon$ and $P^*=(\sigma^3/\varepsilon)P$ and the timescale is given by $\tau=(m\sigma^2/\varepsilon)^{1/2}$ where k_B is the Boltzmann constant, T is the absolute temperature and P is the pressure.

The polymer chain was modelled as a bead-and-spring model. Non-bonded interactions between the polymer beads and between the polymer and solvent particles were also modelled using the Lennard-Jones function of eq. 1. For the intra-chain (polymer-polymer) interactions a cutoff of $r_c = 2^{1/6}\sigma$ was used, while for polymer-solvent interactions two different cutoff distances were employed, depending on whether the solvent solvating the polymer was good or poor (r_c =2.5σ and $r_c = 2^{1/6}\sigma$ respectively). Note that in all cases the interactions between the polymer and both solvent components are identical, i.e. at an interface between two poor or two good solvents.

The polymer topology was maintained through a harmonic potential (V_{bond})

$$V_{bond} = \frac{1}{2}k_l\left(l - l_0\right)^2 \qquad \text{(eq. 2)}$$

where k_l = 250 $\varepsilon\sigma^{-2}$ is the bond stretching force constant, l_0/σ = 1 is the equilibrium bond length and l is the instantaneous bond length. No angular potentials were used so the chains were fully flexible.

The free energy profile (or potential of mean force) was determined using the umbrella sampling technique (US) [20]. The simulations were started with the polymer fully solvated in one of the bulk phases; using the steered molecular dynamics (SMD) method the polymer was then moved towards the interface along a reaction path normal to the interface (z). The starting US configurations were then taken from the SMD trajectories. In each US window

the distance between the centre of mass (CoM) of the polymer and of the solvent was restrained in the z direction using a harmonic potential

$$V_{umb} = \frac{1}{2} k_u \left(z - z_i\right)^2 \quad \text{(eq. 3)}$$

where z is the separation between the centre of mass of the polymer and solvent component A, z_i is the equilibrium distance and k_u is the force constant, whose value was varied from 5 to 20 $\varepsilon\sigma^{-2}$ depending on the distance of the polymer from the interface (in general, high values of k_u were necessary when the polymer was relatively close to the interface in order keep the polymer CoM in the reference position). Finally, the Weighted Histogram Analysis Method (WHAM) [20] was applied to combine the probability distributions from the restrained simulations and construct a free energy profile. In the plots of the free energy profile and polymer structural parameters reported below the z-coordinate has been shifted so that the free energy minimum (which defines the position of the interface) is at z=0.

All simulations were performed using the GROMACS simulation package version 4.5.4 [21] in the NPT ensemble with reduced temperature and pressure of T^*= 1 and P^* = 1 respectively. Temperature and pressure were controlled using a Nose-Hoover thermostat and barostat [22], with relaxation times of 0.5τ for both temperature and pressure. A timestep of 0.005τ was used throughout. Periodic boundary conditions were applied in all three directions.

3. Results

3A. Effect of the polymer molecular weight, topology and solvent quality on the polymer-interface interaction and polymer structure

Shown in Figure 1 are the free energy profiles for the linear and star polymer models (the labels used are as given in Table 1) in poor solvent (Fig 1(a) and (b)) and good solvent (Fig. 1(c) and (d)), while Table 2 reports the values of free energy (FE) of desorption along with their standard errors. In all cases the polymer-interface interaction is attractive, showing that even chemically homogeneous polymers are interfacially active. It should be noted here that the two solvents are chemically identical, so the difference in free energy represents the propensity of the polymer chain to reside at the interface rather than in bulk. The fact that the polymer adsorbs at the interface between two good solvents is in agreement with previous simulation work on dendrimers and nanoparticles. Generally nanoparticles or polymers may be expected to adsorb on the interface if the interfacial tension between the polymer and the solvent is lower than that between the two solvent components.

	FE_{calc}/k_BT	
Model	**Poor solvent**	**Good solvent**
L25	39.5±0.8	29.6±0.8
L40	51.9±0.6	47.0±0.3
L50	59.1±0.9	56.4±0.7
L60	65.4±1.3	64.0±0.6
L70	70.7±0.6	76.5±1.2
L80	76.3±0.5	--
L91	83.2±0.2	--
N4L6	40.1±0.8	28.5±1.1
N6L4	39.4±1.2	25.3±1.2
N11L6	68.6±0.4	56.9±0.4
N6L11	69.4±0.2	70.3±0.8

Table 2. Desorption free Energy (FE) for all the polymers as calculated from simulations. In the table, linear polymer models are labelled as Lx, star polymer models as NyLx (see also Table 1)

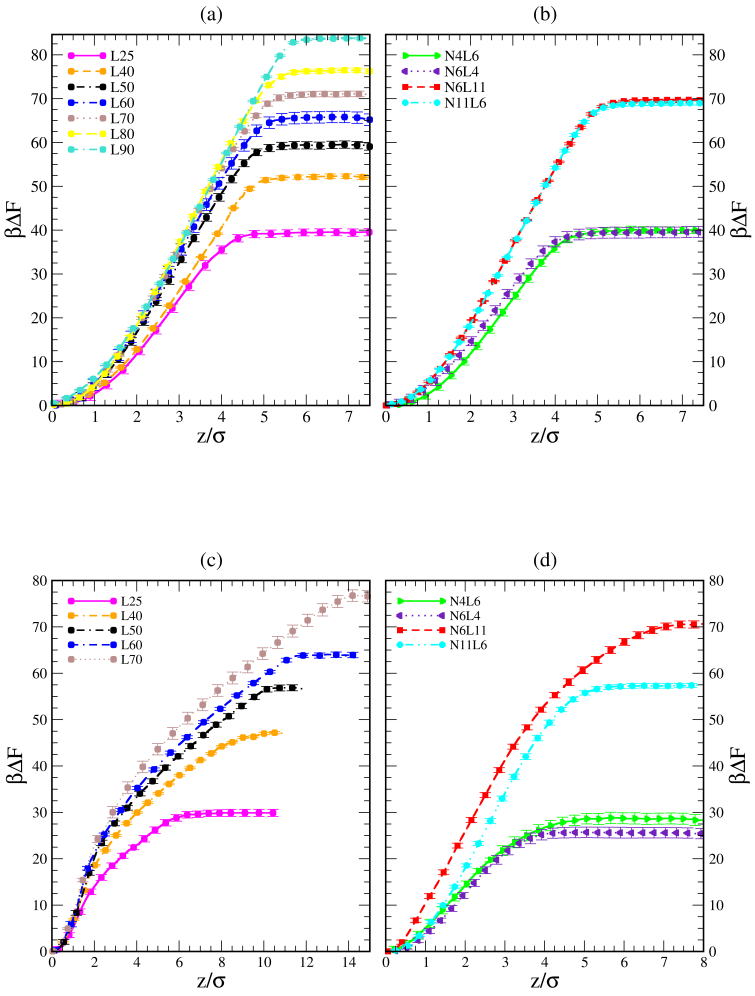

Figure 1. Free energy profiles for linear polymer and star polymer models in poor (a and b) and good solvent (c and d). Labels are explained in Table 1.

Poor solvent. First we shall focus on the poor solvent case for which the free energy profile is found to be only weakly dependent on the polymer topology. The linear polymer with 25 monomers in the chain (L25) shows a FE of desorption very similar to that of the two star polymers with the same M_w (N4L6 and N6L4) and a comparable behaviour is shown by the largest M_w models studied (L70 and the corresponding star polymers N6L11 and N11L6). This insensitivity to the molecule topology may be understood by considering that in a poor solvent the polymer adopts a compact, globular structure to minimise unfavourable polymer-solvent interactions. The structure of the polymers may be quantitatively analysed through the calculation of its radius of gyration (R_g) which is defined as the trace of the gyration tensor ($\mathbf{R}^2$):

$$R^2_{\alpha,\beta} = \frac{1}{N}\sum_{i=1}^{N}(\mathbf{r}^i_\alpha - \mathbf{r}^c_\alpha)(\mathbf{r}^i_\beta - \mathbf{r}^c_\beta);\ \ \alpha,\beta = x,y,z \qquad \text{(eq. 4)}$$

where N is the number of beads in the polymer, r^i_α is the position of the *i*th bead and r^c_α is the position of the polymer CoM.

$$R^2_g = \mathrm{tr}(\mathbf{R}^2) = \lambda_1^2 + \lambda_2^2 + \lambda_3^2 \qquad \text{(eq. 5)}$$

where λ_i (*i*=1,2 and 3) are the principal moments of the gyration tensor and represent the characteristic lengths of the equivalent ellipsoid which describes the macromolecule. Shown in Figures 2a, 2c and 2e are the radii of gyration ($R_g = \sqrt{R^2_g}$) and their components along the *x*, *y* and *z* axis ($\sqrt{R^2_{\alpha,\beta}}$ with α=β) for selected linear and star polymers in poor solvent as a function of the polymer-interface distance (for clarity only the largest molecular weight models are reported but all the other models show the same behaviour, see Figure 1S(a) in the supporting information). As expected, irrespectively of the polymer topology (or molecular weight; see supporting information in Figure 1S) the polymer overall size changes only slightly with polymer-interface separation. Close to the interface the molecule radius of gyration is slightly higher than in bulk, due to the swelling of the polymer in the low density interfacial region, and starts to decrease towards the bulk value at around z=4-5σ (depending on the polymer M_w). For distances above ≈5σ, the molecule size becomes stable and reaches its bulk values (reported in Table 1S for all the linear polymers investigated).

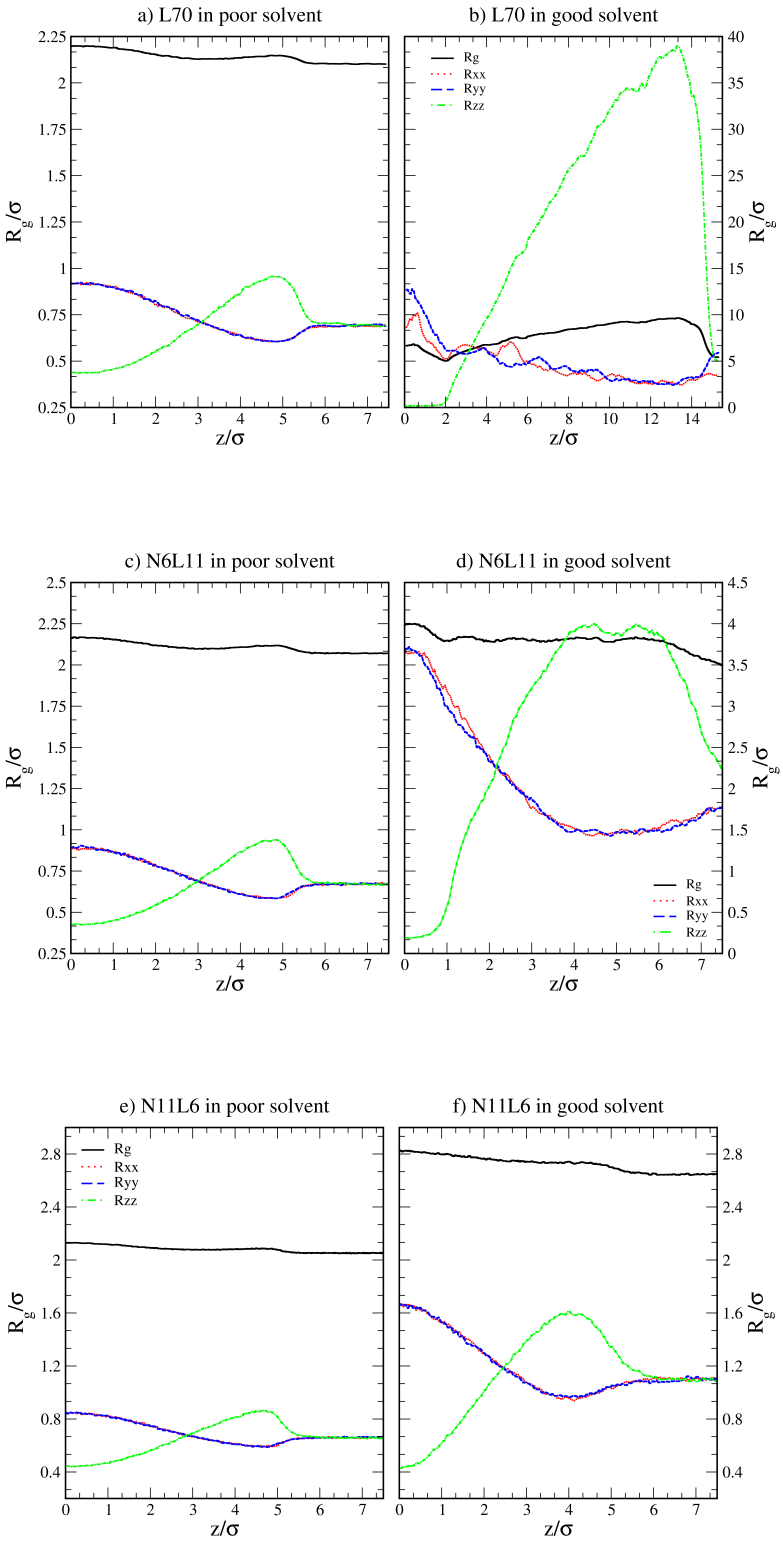

Figure 2. Radius of gyration (R_g) and its components in the *x, y* and *z* directions (R_{xx}, R_{yy} and R_{zz}) for linear polymer L70 and star polymers homologues N6L11 and N11L6 in poor and good solvents.

More insight into the change in the 3D shape of the macromolecule can be gained by looking at the three different components of the radius of gyration: R_{xx}, R_{yy} and R_{zz} (Figure 2). The plot shows that at the interface the macromolecule assumes a disk-like shape ($R_{zz} << R_{xx} = R_{yy}$). Moving away from the interface, the polymer changes shape stretching towards the interface ($R_{zz} > R_{xx} = R_{yy}$) until it takes the unperturbed globular conformation ($R_{zz} = R_{xx} = R_{yy}$) when in bulk. These changes in the macromolecule shape can be quantified by calculating the structural parameters K_1 and K_2 [23] defined as $K_1 = (<\lambda_2> + <\lambda_3>)/(<\lambda_1> + <\lambda_2>)$ and $K_2 = (<\lambda_1> + <\lambda_3>)/(<\lambda_1> + <\lambda_2>)$ where $\lambda_1 \geq \lambda_2 \geq \lambda_3$. Figure 3 reports the values of K_1 and K_2 as a function of the distance from the interface for L70 and the corresponding star polymers, N6L11 and N11L6.

As expected the change in molecule shape is only subtle but it is now possible to observe that the value of z at which the maximum in the R_{zz} occurs corresponds to the separation at which the polymer changes from approximately spherical ($K_1=K_2=1$) to a more elongated shape (an infinite thin rod corresponds to $K_1=0$ and $K_2=1$). Due to the compact shape of the macromolecules, their free energy profiles are very similar to that found for nanoparticles [18, 24]; specifically the interaction is relatively long-ranged (larger than the polymer R_g), in part due to broadening of the interface by thermal capillary waves, and the free energy increases smoothly before plateauing when in the bulk. As it will be discussed later, the similarity between the free energy profiles of polymers of different topologies originates from the fact that the molecule adopts a compact shape, screening the internal monomers from the solvent. Therefore, only the external monomers, those exposed to the solvent interactions, contribute to the calculated FE values. Finally, it can be seen that in the bulk solution the radius of gyration for the different linear polymers increases with the polymer M_w (see table S1 in the supporting information), following the scaling law $R_g \propto M_w{}^{v}$, with a Flory exponent v=0.33 in agreement with the theory [25].

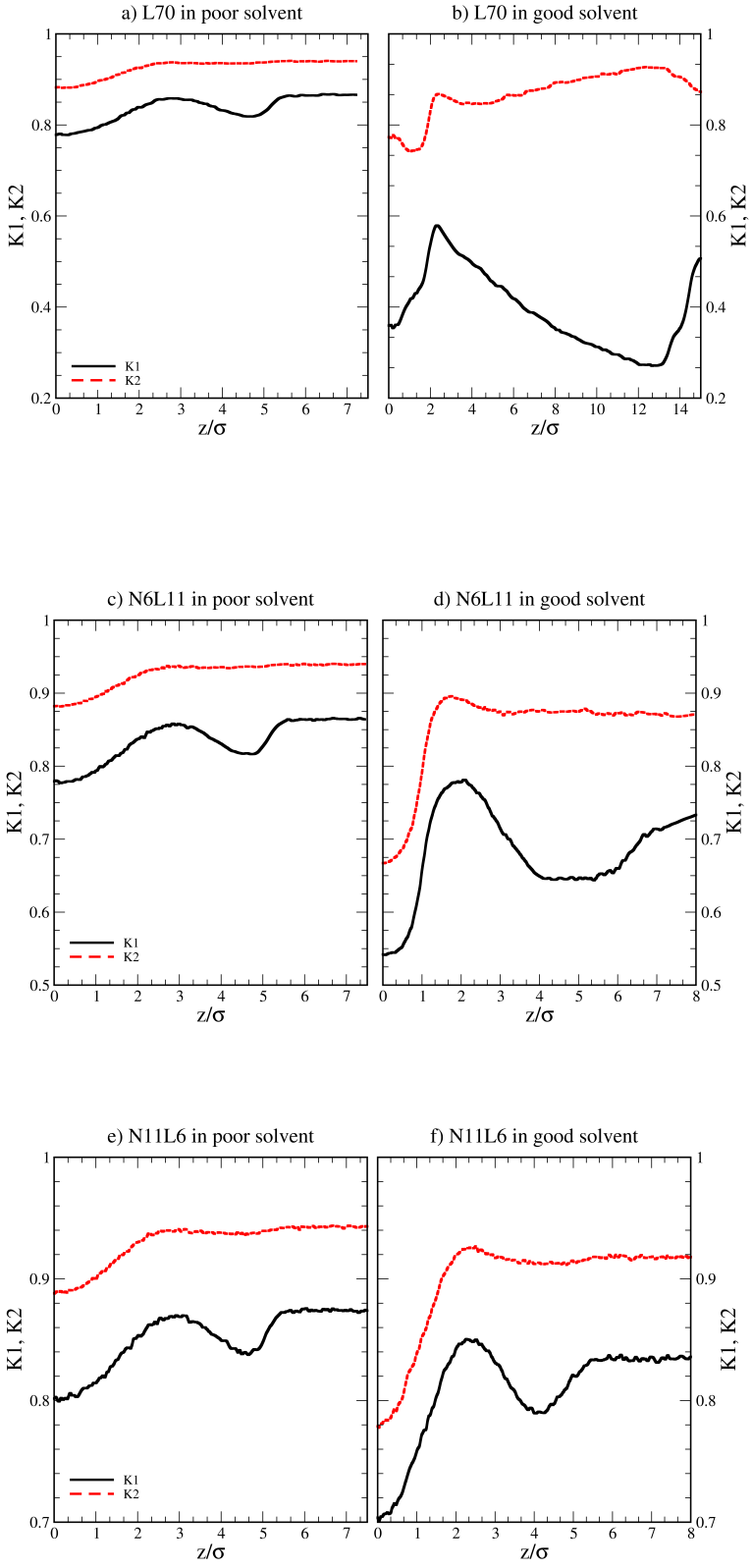

Figure 3. Structural parameters K_1 and K_2 for linear polymer L70 and star polymer homologues N6L11 and N11L6 in poor and good solvent.

Good solvent. In the good solvent case, the free energy profile shows a much stronger dependence on the molecule topology (Figure 1(c) and (d)). In particular, for the linear polymers the free energy varies sharply at small polymer-interface separations and acquires a long-ranged tail, which becomes more evident as the chain length increases. This long-range polymer-interface interaction is due to the fact that the polymers, especially the linear ones, can adopt an extended configuration reaching to the interface even if the polymer lies fairly far from it (see Figures 2 (b) and 2S in the supporting information). When the arms become long enough this effect is also evident for the star polymers (i.e. N6L11) (see Figure 2(d) and (f)). In contrast to the poor solvent case, in good solvent all linear polymers show a remarkable change in radius of gyration as a function of their distance from the interface (Figure 2(b)). Irrespective of the polymer M_w (see Figure 2S in the supporting information), there is a drop in the size of the polymer at short polymer-interface separation (within 2σ) followed by a steep and monotonic expansion of the chain. This corresponds to an initial sharp increase in FE of desorption (see Figure 1(c)). For the linear polymers and for the star polymer with the longest arms (N6L11), although less pronounced, the initial reduction of the polymer size at close distance from the interface is due to a compression of the molecule in only the x and y directions (i.e. R_{zz} remains constant). This compression is associated with an immediate quick increase in the FE (see Figure 1c $0 < z \leq 2\sigma$). The steep increase in the R_g that follows at larger distances is due to the elongation of the polymer chain in the direction perpendicular to the interface (z) and to a simultaneous slight compression in only the x and y directions. These changes can again be better quantified by looking at the structural parameters K_1 and K_2 in Figure 3(b), (d) and (f)). The values clearly indicate that linear and star polymers undergo a sequence of shape changes: elongated, $K_2 >> K_1$ (linear models) or disk-like, $K_1 \approx K_2 \approx 0.5$ (star models) at the interface to maximise the reduction in interfacial area between the solvent components, and rod-like at intermediate separations ($K_1=0$ and $K_2=1$), allowing part of the polymer to remain in contact with the interface (again reducing the interfacial area) (see also snapshots in Figure 4). These results clearly show that the biphasic system favours a conformation where the polymer resides at the interface and, despite an entropic and enthalpic penalty, forces the chain to stretch towards it. Furthermore, At the polymer-interface distance at which the FE reaches a plateau, the polymer R_g starts to decrease until the bulk value (always slightly smaller than that observed at the interface) is obtained. The R_g of polymers in bulk are reported in Table 1S of the supporting information. The Flory parameter, v, calculated for linear polymers in the good solvent is equal to 0.59 in agreement with the theory [25]. The shape changes as a function of z for star polymers with short arms are less pronounced since the conformational space available is much more restricted (Figures 2(f) and 3(f)). Indeed, high M_w star polymers with short arm (i.e. N11L6)

show lower desorption FE than star polymers with the same M_w but longer arms (i.e. N6L11), indicating that they are less stable at the interface than their homologues with longer arms.

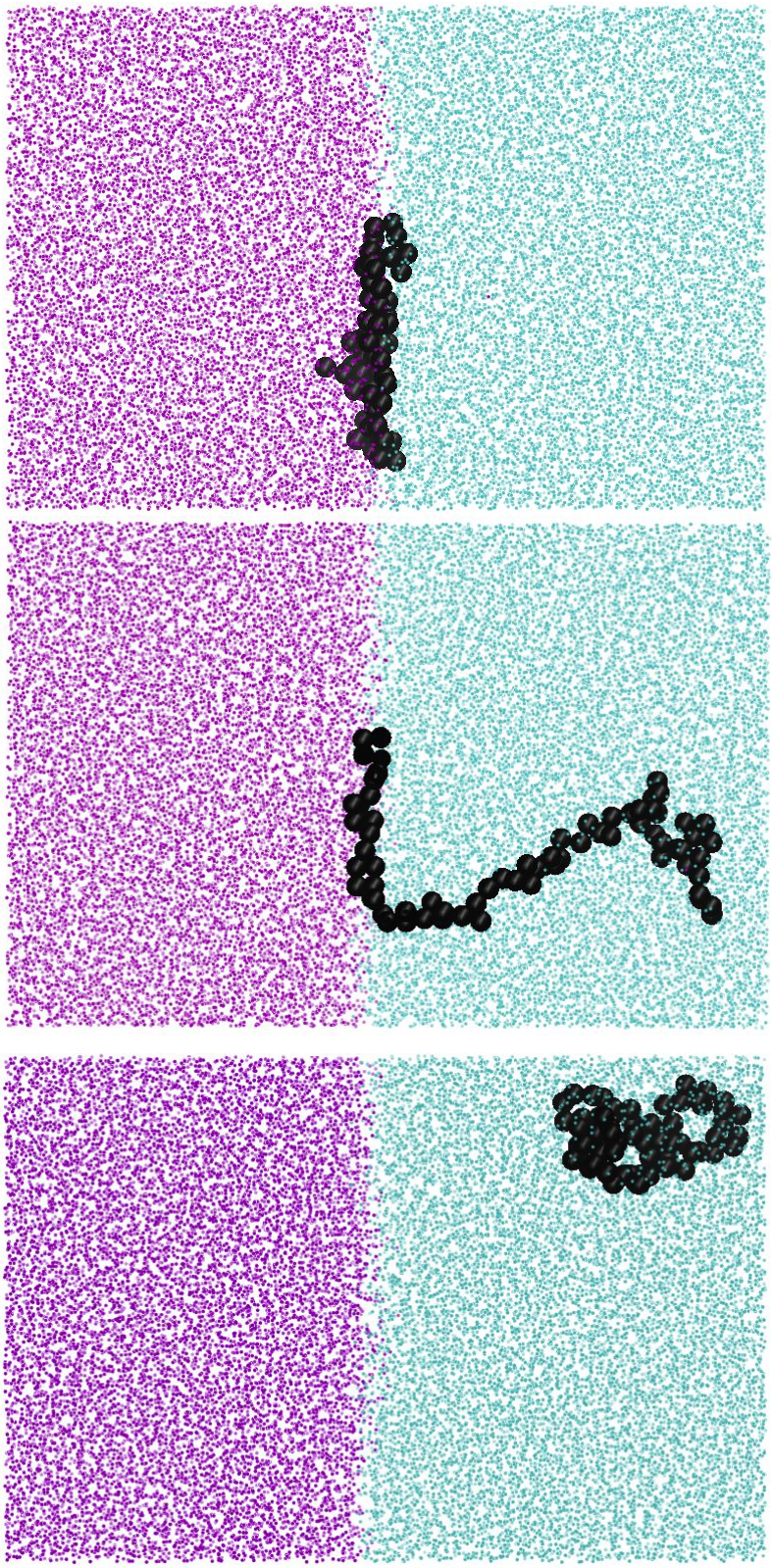

Figure 4. From the top: simulation snapshots showing L70 at the interface, at intermediate distance from interface and in bulk in good solvent.

3.B Calculated desorption free energy

The influence of the macromolecules conformational freedom on their stability at the interface is highlighted in Figure 5, where the values of the desorption free energies reported in Table 2 are plotted against the polymer M_w. As expected, the FE of desorption increases with the polymer M_w, with this trend being more evident in good solvent than in poor solvent. As already noted, the length and number of arms in the star polymers affect the corresponding FE values only in good solvent and only for high M_w polymers. Moreover, since in good solvent the FE values increases more rapidly with the polymer M_w, for a long enough linear polymer chain, the FE of desorption in good solvent overtakes the value obtained for the same polymer in poor solvent. A similar effect can be also noticed for the star polymers where, when the arms are long enough (namely for N6L11) the desorption FE becomes comparable with that obtained in poor solvent for same M_w.

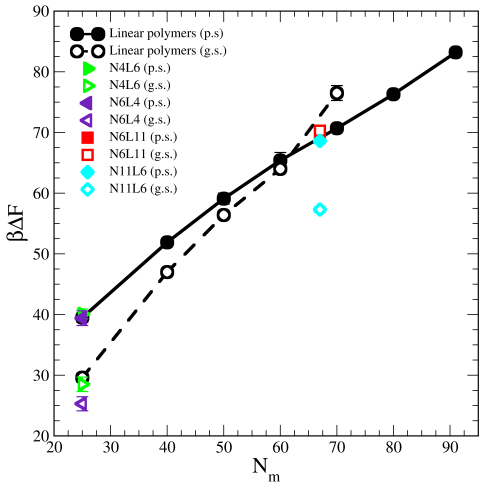

Figure 5. Desorption free energies for star and linear polymers. Data for poor and good solvents denoted by filled and open symbols respectively. In the legend p.s. stays for poor solvent and g.s. for good solvent.

In order to understand the desorption strength it is useful to decompose it into separate contributions. In particular three contributions may be calculated: (i) the change in the interfacial area between the two solvent components and the resulting change in interaction energy, (ii) the change in polymer-solvent interaction energy between the polymer in bulk solution and at the interface, and (iii) the change in polymer entropy.

The first contribution (change in interfacial area between the two solvents) has often been

invoked to understand the adsorption of colloids and nanoparticles onto fluid interfaces. In this case the free energy of the colloid at the interface is often expressed as [26]

$$FE = \gamma_{12}A_{12} + \gamma_{1P}A_{1P} + \gamma_{2P}A_{2P} \qquad \text{(eq. 6)}$$

where γ_{ij} (i, j = 1, 2, *P* where 1 and 2 corresponds to any of the two solvent components and *P* stays for polymer) are the interfacial tensions and A_{ij} are the surface areas. The desorption free energy is then given by the difference between FE of the polymer in bulk solution and the FE obtained in eq. 6

$$\Delta F_i = \gamma_{12}A_{12} + \gamma_{iP}A_P - \left(\gamma_{12}A'_{12} + \gamma_{1P}A_{1P} + \gamma_{2P}A_{2P}\right) \qquad \text{(eq. 7)}$$

where i this time can assume only the value 1 and 2 and A'_{12} is the change in solvent interfacial area due to polymer adsorption. Now, considering that $A_{12}-A'_{12}$ equal to A_{int}, where A_{int} is the interfacial area occupied by the polymer, that the polymer-solvent interaction is identical for both solvent components, $\gamma_{1P} = \gamma_{2P}$, and assuming that the total surface area of the polymer remains constant ($A_P=A_{1P}+A_{2P}$) the only contributing to the desorption FE in eq. 7 is the solvent/solvent surface tension and the polymer interfacial area (i.e. $\Delta F_i = \gamma_{12}A_{int}$).

The values of the interfacial area (A_{int}) occupied by each polymer are shown in Figure 6(a). This area is calculated as reported in Ref. [19] where the simulation box is sliced perpendicular to the *z* axis and the van der Waals area occupied by the polymer beads belonging to the slice associated with the solvent/solvent interface (z=0) is calculated. As expected the area occupied by the polymer at the interface is larger in good solvent than in poor solvent, and it increases with the polymer M_w. The larger the polymer interfacial area is, the higher the effective screening of the unfavourable interactions between the two solvents (which are responsible of the positive desorption FE values obtained in both solvent cases) becomes. Indeed the trend in interfacial area reported in Figure 6(a) correlates with the fact that the FE increases with the polymer M_w faster in good solvent than in poor one. The effect of the polymer topology can be as well understood from Figure 6(a). In good solvent star polymers with short arms (N6L4 and N11L6) show a lower interfacial area compared with their linear homologues and this effect becomes more apparent for larger M_w.

The importance of the screening effect mentioned above is even more clear in Figure 6(b) which shows that the major enthalpic contribution to the desorption free energy is given by

the solvent-solvent interaction (ΔE_{ss}). Indeed, for both poor and good solvent cases the difference in intermolecular energy is positive (i.e. the system favours configurations with the polymer at the interface) and of the order of hundreds of k_BT. The values of ΔE_{ss} also follow the same trend with the polymer M_W and topology as that shown by the FE, increasing with the number of monomers along the chain for the linear polymers and with the length of the arm for the star ones. Finally, as in the FE case, ΔE_{ss} increases with the polymer M_w more rapidly in good solvent than in poor solvent. The values obtained for ΔE_{ss} are, however, higher than the calculated FE, indicating that other contributions reducing the stability of the polymer at the interface play a role.

One of these contributions is the difference in polymer-solvent interaction energy (ΔE_{ps}) between polymers in bulk solution and at the interface shown in Figure 6(c). In poor solvent ΔE_{ps} is small (of the order of k_BT) and positive while in the good solvent ΔE_{ps} is of the order of tens of k_BT and is negative. These results can be understood observing that at the interface the solvent density is lower than in bulk (see Figure 7) and therefore the number of polymer/solvent contacts are minimised when the polymer is absorbed at the interface. In poor solvent this reduction in the number of contacts leads to a slight stabilisation of the polymer at the interface. Instead in good solvent, it leads to an increase of the energy of the system which prefers to have the polymer surrounded by the highest possible number of solvent beads and therefore favours the configuration where the polymer is placed in bulk. In good solvent ΔE_{ps} shows indeed an opposite trend with the polymer M_w and topology than that shown by the values of the FE: ΔE_{ps} decreases with the number of monomers (i.e. the higher is the M_w, the less favourable is the configuration where the polymer is at the interface) and with the number of arms (N11L6 is the polymer with the lowest ΔE_{ps} (-26.3 k_BT) among the star polymers).

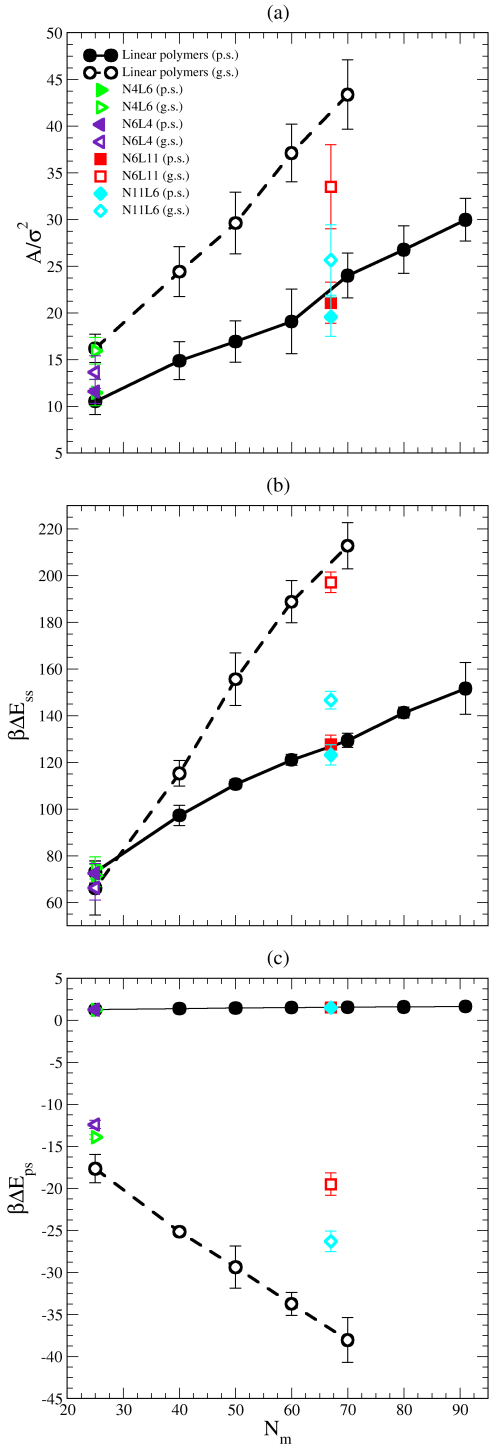

Figure 6. a) Polymer interfacial area. Data for poor (p.s. in the legend) and good (g.s. in the legend) solvents denoted by filled and open symbols respectively, b) Difference in solvent-solvent interaction energy between the configuration with the polymer in the bulk and at the interface. Symbols as in (a). c) Difference in polymer-solvent energy between the configuration with the polymer in bulk and at the interface. Symbols as in (a).

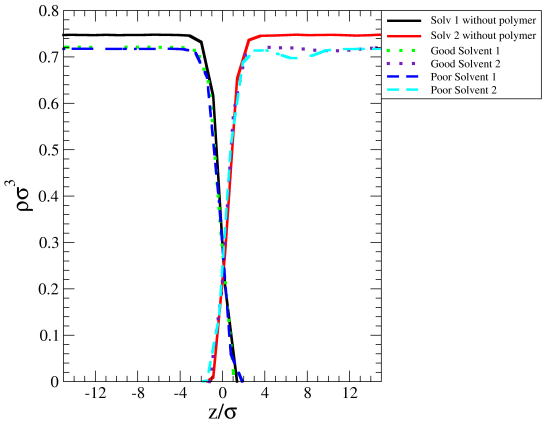

Figure 7. Solvent and polymer (L70) density profile calculated across the simulation box for poor and good solvent. The solid lines denote the profiles calculated for a system without the polymer. In the poor solvent case (light blue dashed line) the small peak in the distribution visible in proximity of the interface represents the polymer beads. In good solvent (dotted magenta line) the polymer chain assumes an extended conformation and its beads are delocalized along the interface.

The contribution from the entropy change is harder to estimate than the previous terms. Assuming that the polymer translational entropy change is negligible, the change in entropy due to the adsorption of the chain into the interface is mainly due to a change in its conformational entropy (S_c). Knowing all the possible microstates (i.e. configurations) accessible to the polymer chain, the value of S_c can be evaluated using the Gibbs entropy equation

$$S_c = -k_B \sum P(R) \ln P(R) \qquad \text{(eq. 8)}$$

where k_B is the Boltzmann constant, R is the chosen molecular descriptor which in our case is the end-to-end distance distribution (the radius of gyration could also been used [27]), and $P(R)$ is the probability distribution of the polymer end-to-end distance, which in case of the star polymer is calculated as the average distance between the end monomers of two arms. The calculated values of $\Delta S_c = S_c^b - S_c^i$, where S_c^b and S_c^i are the conformational entropy values for the polymer in bulk and at the interface respectively, are plotted in Figure 8. For both poor and good solvents the conformational entropy at the interface is larger than in bulk solution ($\Delta S_c < 0$) since the polymer expands at the interface due to the depletion region between the two solvents as seen in Figure 7 allowing the polymer chain to explore more configurations. It can be seen, however, that in both solvents the values of ΔS_c are very small, indicating that the change in polymer conformational entropy does not play a significant role in the

thermodynamics of the adsorption of macromolecules at the interface. As expected the longer the polymer chain is, the larger is the change in conformational entropy, so ΔS_c becomes more negative. It is also interesting to notice that from our calculations it appears that star polymers have similar if not lower conformation entropy than their linear homologues maybe due the fact that the arms are shorter than the corresponding linear polymers (11 monomers against 70 monomers in the case of N6L11 and L70 respectively).

For both poor and good solvents, it is expected that the solvent entropy will increase when the polymer is at the interface, which as we will see in the next section, seems to be the case.

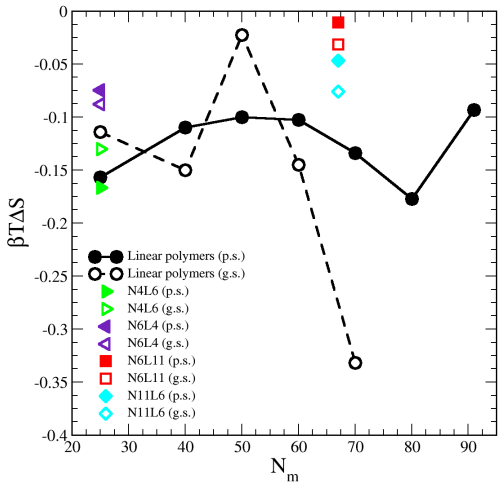

Figure 8. Change in polymer conformational entropy. Data for the poor (p.s.) and good (g.s.) solvents denoted by filled and open symbols respectively.

3C. Prediction of the desorption free energy from bulk simulations

Computationally, the prediction of the FE values for processes involving macromolecules is very time consuming. Each configuration featuring the polymer chain at a specific spatial position needs to be simulated for a long time in order to collect enough data to obtain FE values with small statistical uncertainty. Experimentally the collection of thermodynamic data such as partition coefficients or solubility parameters for polymer solutions is also time consuming and it is a common practice to resort to contribution theory methods. This involves measuring a specific thermodynamic property for a small molecule that resembles the polymer monomer and the same property is estimated for the polymer assuming additivity [28]. Although this procedure is attractive since it is simple and the data for small organic molecules are often widely available, the approach does not always provide accurate results [29]. Indeed the assumption that all monomers of the polymer chain contribute equally to the

polymer properties is not always correct. Our FE data suggests that this is not true, especially for a polymer dissolved in poor solvents. Here monomers which are buried inside the polymer 'blob' do not interact with the solvent molecules and therefore do not contribute to the calculated FE. Indeed if the FE values reported in Table 1 are normalised by the number of polymer monomers, it is not possible to obtain a constant value indicating that not all the monomers contribute to the desorption FE. Here, we attempt to predict the FE values obtained with the umbrella sampling technique using data available from short simulations of polymers in bulk solution.

Firstly we combine the separate contributions calculated in the previous section. We then obtain the following equation

$$\Delta F_{pred} = \Delta H - T\Delta S = \gamma_{ss} A_{int} + \Delta E_{ps} - T\Delta S_p$$

(eq. 9)

In this relation we neglect the change in solvent configurational entropy (ΔS_s), which we haven't calculated. Our predicted FE values therefore contain the contribution coming from the solvent/solvent interaction screened by the presence of the polymer ($\gamma_{ss} A_{int}$) where A_{int} is the polymer interfacial area (Figure 6(a) and γ_{ss}=1.54 $k_B T\sigma^2$ is the interfacial tension calculated from the difference between the normal and transverse pressures ($\gamma_{ss}=(L/2)(P_N - P_T)$), the polymer/solvent enthalpic contribution (ΔE_{ps}) (Figure 6(c)) and the polymer conformation entropy change (ΔS_p) (Figure 8). In Figure 9 the value of the predicted (using eq. 9) desorption free energy are plotted against the polymer M_w. As it can be seen the predicted FE values are consistently smaller than the calculated one. The difference between the calculated and predicted FE values increases with the polymer M_w and is larger in the good solvent than in the poor solvent. The underestimation of the FE obtained from eq. 9 might therefore be ascribed to the neglected contribution of the solvent entropy, which seems to play a crucial role in the determination of the FE values. Although eq. 9 cannot quantitatively predict the FE values, it can qualitatively predict their dependence with the chain topology and, less accurately, on the M_w. Indeed, the predicted FE values in poor solvent are not affected by the polymer topology, and the dependence on the length of the polymer arms is only visible in good solvent (although we should notice that the predicted values underestimate this dependence). The FE increases with the polymer M_w but this increase is less than calculated from simulation, in particular for the good solvent case.

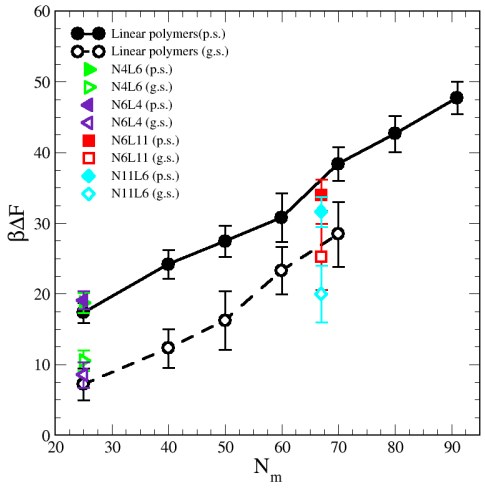

Figure 9. Predicted adsorption free energy for the star and linear polymers using eq. 9. Data for poor (p.s.) and good solvent (g.s.) denoted by filled and open symbols respectively.

Considering that the magnitude of the FE of desorption depends on the interaction between the polymer and the solvent, another approach that can be followed to predict its trend is to take into account the polymer solvent accessible surface area (*SASA*). A dependence on the SASA may be expected, as only the polymer beads near the surface will contribute to the polymer solvent interaction and the number of surface beads is reasonably approximated by the SASA. This approach is akin to that used to develop implicit solvent models for biological macromolecules and more recently applied also on model polyelectrolytes where the *SASA* values are used to calculate the solvation free energy. [30, 31]

We then calculate the *SASA* for each polymer (linear and star) in bulk of both good and poor solvents using a probe with a radius identical to that of the solvent bead using the analytical method proposed by Eisenhaber et al. [32] and implemented in the program g_sas of GROMACS [21]. The resulting *SASA* values are reported against the corresponding FE data in Figure 10 where the values of the FE calculated for a single bead in both solvents and the corresponding *SASA* (calculated analytically) are also reported. As can be seen there is a perfect correlation between the values of *SASA* and those of the corresponding desorption FE for all systems simulated irrespectively to the topology of the polymer. The predicted FE using this approach can be therefore calculated as

$$\Delta F_{pred} = \Delta F^{b} \times SASA \quad \text{(eq. 10)}$$

where ΔF^{b} is the FE calculated for a single bead using the umbrella sampling technique and

normalised by the bead surface area. The FE values predicted using the *SASA* method are reported in Figure 11. As it can be seen the actual FE values are overestimated this time but the trend of the FE with the polymer M_w and topology is reproduced very well. This result seems to indicate that the FE of desorption of a homopolymer at a solvent/solvent interface might be qualitatively predicted by knowing its solvent accessible surface in bulk and calculating the FE only for its monomer bead. It is worth stressing that in this model system the solvent quality for the binary mixture is identical and some adjustments may be needed to eq. 10 when applied to more realistic systems.

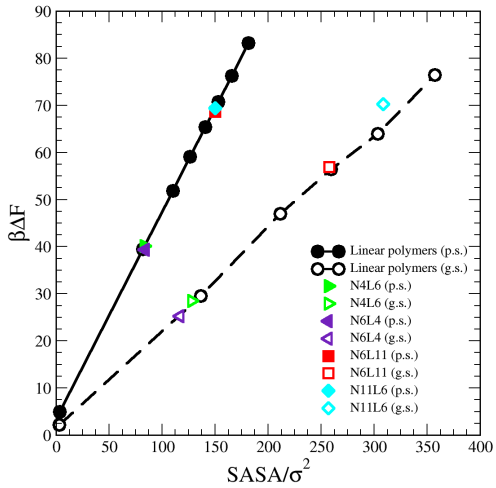

Figure 10. Solvent Accessible Surface Area (*SASA*) calculated for polymer models reported in Table 1 against the corresponding calculated free energy values. Data for poor (p.s.) and good (g.s.) solvent denoted by filled and open symbols respectively.

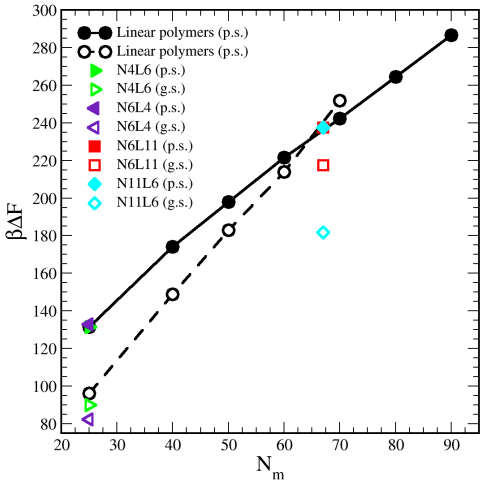

Figure 11. Predicted free energy values calculated using equation 10. Data for poor (p.s.) and good solvent (g.s.) denoted by filled and open symbols respectively.

Summary and Conclusions

The understanding of the behaviour of macromolecules near fluid interfaces is vital in order to control and design new interfacial processes such as those occurring in foams or emulsions. Very little it is known on the thermodynamics of these interfacial systems and on the effect that the topology of the macromolecules has on their stability. By means of a simplified model we have been able to start to reveal the basic thermodynamic contributions to the polymer adsorption strength and correlate them to the polymer structural properties.

We found that in all the cases analysed the homopolymer acts as surface active molecule, showing a propensity to reside at the interface. In common with nanoparticles and dendrimers this demonstrates that, irrespectively to the nature of the solvent, explicit amphiphilicity is not necessary for surface active species.

We noticed that the desorption free energy increases with the polymer molecular weight in both poor and good solvents but in the latter this increase is more rapid than in the former. For high molecular weight linear polymers this increase leads to a desorption free energy which is higher in good solvent than in poor solvent. Moreover we observed that the polymer topology affects the interfacial stability of the macromolecule only in good solvent and for star polymers with long arms.

We explain these findings in terms of polymer structural changes. Calculating the three components of the radius of gyration along the x, y and z axes and the eigenvalues of the gyration tensor, we find that the polymer chain undergoes few conformational changes moving away from the interface. These conformational changes are more evident in good solvent than in poor one. In both cases these structural changes act to decrease the interfacial area between the two immiscible solvents. In particular, in good solvent, when at the interface, the polymer occupies as much area as possible helped also by an increased conformational freedom due to a reduced solvent density. Away from the interface the chain extends and assumes a two domain structure where one of the domains is still in contact with the interface. Similar structural changes, although less evident, occur also in poor solvent and it is possible to correlate them to the free energy profiles.

In order to determine the factors that control the adsorption strength at the interface, we have evaluated different contributions to the desorption free energy. The largest contribution arises from the decrease in interfacial area between the two immiscible liquids caused by the adsorption of the polymer at the interface. This is similar to the mechanism by which

nanoparticles adsorb at liquid interfaces. The stability of the polymer at the interface is counterbalanced, in good solvent, by the favourable interactions between the polymer and the solvent in bulk, leading to a significant decrease in free energy. We also showed that the polymer conformational entropy represents a very small contribution to the total free energy of the system.

Finally, we attempted to predict the desorption FE using data obtained from bulk simulations. We found that the solvent entropy seems to be a major contributor to the desorption FE and predictions neglecting this term lead to an underestimation of its value. If we instead use the data related to the polymer solvent accessible surface area calculated in bulk, the predicted FE (although the actual numbers are higher than the calculated values), follow the expected trend with the polymer M_w and topology. This opens the possibility of devising a novel and simple method to predict the stability of polymers at fluid interfaces without performing time consuming calculations. Work to investigate the applicability of this method to chemically detailed systems is currently on going.

Acknowledgements

This work was partially funded by the Leverhulme Trust (ECF/2010/2054). Computational facilities for this work were provided by the Centre for Scientific Computing, University of Warwick and the Computer Shared Facility, University of Manchester.

References

1. C. N. R. Rao, G. U. Kulkarni, V. V. Agrawal, U. K. Gautam, M. Ghosh and U. Tumkurkar, *J. Colloid Interface Sci.*, 2005, **289**, 305-318.
2. L. Hu, M. Chen, X. Fang and L. Wu, *Chem. Soc. Rev.*, 2012, **41**, 1350-1362.
3. P. W. Morgan, *Interfacial Polymerization*, John Wiley & Sons, Inc, 2011.
4. K. Landfester, *Angewandte Chemie-International Edition*, 2009, **48**, 4488-4507.
5. D. Quintanar-Guerrero, E. Allemann, H. Fessi and E. Doelker, *Drug Dev. Ind. Pharm.*, 1998, **24**, 1113-1128.
6. N. Di Pasquale, D. L. Marchisio, P. Carbone and A. A. Barresi, *Chem. Eng. Res. Des.*, 2013, **91**, 2275-2290.
7. M. Redhead, G. Mantovani, S. Nawaz, P. Carbone, D. C. Gorecki, C. Alexander and C. Bosquillon, *Pharm. Res.*, 2012, **29**, 1908-1918.
8. S. Nawaz, M. Redhead, G. Mantovani, C. Alexander, C. Bosquillon and P. Carbone, *Soft Matter*, 2012, **8**, 6744-6754.
9. K. Inoue, *Prog. Polym. Sci.*, 2000, **25**, 453-571.
10. X. Guo, M. Baumgarten and K. Mullen, *Prog. Polym. Sci.*, 2013, **38**, 1832-1908.
11. J. N. Liu, H. E. Duong, M. R. Whittaker, T. P. Davis and C. Boyer, *Macromol. Rapid Commun.*, 2012, **33**, 760-766.
12. S. Kienle, M. Gallei, H. Yu, B. Zhang, S. Krysiak, B. N. Balzer, M. Rehahn, A. D. Schluter and T. Hugel, *Langmuir*, 2014, **30**, 4351-4357.
13. K. Johnston and V. Harmandaris, *Macromolecules*, 2013, **46**, 5741-5750.
14. R. D. Priestley, C. J. Ellison, L. J. Broadbelt and J. M. Torkelson, *Science*, 2005, **309**, 456-459.
15. R. A. L. Jones and R. W. Richards, *Polymers at surfaces and Interfaces*, Cambridge University Press, 2006.
16. A. Halperin and P. Pincus, *Macromolecules*, 1986, **19**, 79-84.
17. D. L. Cheung and P. Carbone, *Soft Matter*, 2013, **9**, 6841-6850.
18. D. L. Cheung and S. A. F. Bon, *Phys. Rev. Lett.*, 2009, **102**, 066103-066107.
19. S. Nawaz and P. Carbone, *J. Phys. Chem. B*, 2011, **115**, 12019-12027.
20. S. Kumar, D. Bouzida, R. H. Swendsen, P. A. Kollman and J. M. Rosenberg, *J. Comput. Chem.*, 1992, **13**, 1011-1021.
21. B. Hess, C. Kutzner, D. van der Spoel and E. Lindahl, *J. Chem. Theory Comput.*, 2008, **4**, 435-447.
22. H. J. C. Berendsen, J. P. M. Postma, W. F. van Gusteren, A. Di Nola and J. R. Haak, *J. Chem. Phys.*, 1984, **81**, 3684-3690
23. V. A. Ivanov, M. R. Stukan, V. V. Vasilevskaya, W. Paul and K. Binder, *Macromol. Theo. Sim.*, 2000, **9**, 488-499.
24. D. L. Cheung, *J. Chem. Phys.*, 2011, **135**, 51704.
25. M. Rubinstein and R. H. Colby, *Polymer Physics*, Oxford University Press, 2003.
26. F. Bresme and M. Oettel, *J. Phys.-Cond. Mat.*, 2007, **19**, 413101-413134.
27. S. R. Euston, *Biomacromolecules*, 2010, **11**, 2781-2787.
28. B. A. Miller-Chou and J. L. Koenig, *Prog. Polym. Sci.*, 2003, **28**, 1223-1270.
29. B. C. Lee and R. P. Danner, *Aiche J.*, 1996, **42**, 837-849.
30. J. Kleinjung and F. Fraternali, *Curr. Opin. Struc. Bio.*, 2014, **25**, 126-134.
31. G. Reddy and A. Yethiraj, *J.Chem. Phys.*, 2010, **132**, -.
32. F. Eisenhaber, P. Lijnzaad, P. Argos, C. Sander and M. Scharf, *J. Comput. Chem.*, 1995, **16**, 273-284.